frontiers | Frontiers in Marine Science

TYPE Original Research
PUBLISHED 11 January 2024
DOI 10.3389/fmars.2023.1292802

OPEN ACCESS

EDITED BY
Cheng Zhang,
South China University of Technology, China

REVIEWED BY
Yi Zhong,
Southern University of Science and Technology, China
Qiong Wu,
Hohai University, China
Ning Fan,
Wenzhou University, China

*CORRESPONDENCE
Chen-Feng You
cfy20@mail.ncku.edu.tw

RECEIVED 12 September 2023
ACCEPTED 14 December 2023
PUBLISHED 11 January 2024

CITATION
You C-F, Liao W-L, Huang K-F, Chung C-H and Liu Z (2024) Sediment source variation using REEs, Sr, and Nd isotopic compositions: a case study in MD05-2901, northwestern South China Sea.
Front. Mar. Sci. 10:1292802.
doi: 10.3389/fmars.2023.1292802

Sediment source variation using REEs, Sr, and Nd isotopic compositions: a case study in MD05-2901, northwestern South China Sea

Chen-Feng You[1*], Wei-Lan Liao[1], Kuo-Fang Huang[2], Chuan-Hisung Chung[1] and Zhifei Liu[3]

[1]Department of Earth Sciences, National Cheng Kung University, Tainan, Taiwan, [2]Institute of Earth Sciences, Academic Sinica, Taipei, Taiwan, [3]State Key Laboratory of Marine Geology, Tongji University, Shanghai, China

The South China Sea (SCS) is the largest marginal sea in the western Pacific, fed by large Asian rivers, characterized by substantial volumes of sediment derived from surrounding Asian continents and islands. This study utilizes the rare earth elements (REEs), Sr isotopes ($^{87}Sr/^{86}Sr$), and Nd isotopes (ε_{Nd}) in detritus fractions of MD05-2901 sediments in northwestern SCS, to evaluate the relative contribution among the Mekong River, the Red River, the Pearl River, and rivers in SW Taiwan over the last 32 ka. This deep-sea core is located off the coast of central Vietnam, an upwelling region with only minor continental inputs, and this study is important for a better understanding of the main sources of terrigenous material and their temporal variations in the region. In addition, potential particle exchange is examined using the same proxies in the Fe-Mn oxyhydroxide fractions. The obtained records are systematically compared with the available climatic archives in the region. The REEs in the Fe-Mn oxyhydroxides support the argument of water mass signature separation in bulk sediments by chemical leaching procedures. These $^{87}Sr/^{86}Sr$ in the Fe-Mn oxyhydroxides phase fall in a range between 0.709262 and 0.709313, deviating significantly from the modern seawater. ε_{Nd} values vary >3ε, being more radiogenic in the Fe-Mn oxyhydroxides, where the lowest value occurred in the Bølling/Allerød (B/A) and higher values occurred during the Younger Dryas (YD). The latter implies increased contribution of loess dusts or Taiwanese rivers under dry/cold climatic conditions, compared with the situation in modern times. The Red River and the Mekong River together may have contributed >60% during the Last Glacial Maximum (LGM) and YD. In contrast, the Pearl River components have increased sharply to ~60% during the warm B/A. These results demonstrate that the MD05-2901 sediments sensitively record changes in weathering intensity on land and transport pathways in the coastal regions in the Holocene.

KEYWORDS

South China Sea, REEs, Sr and Nd isotopes, climatic change, MD05-2901

1 Introduction

The South China Sea (SCS) is the largest marginal sea in the western Pacific, and is located at the junction of the Eurasian, the Pacific, and the Indo-Australian plates (Li et al., 2015). Its central basin, >3,500 m deep, is surrounded by various lands and shallow straits, except the Luzon Strait, which is >2,500 m deep. There are large volumes of sediments discharged to the SCS from major Asian rivers, such as the Mekong River, the Red River and the Pearl River, delivering 160, 130, and 100 × 10^6 t/yr, respectively, to the slope region in the NW SCS, as well as rivers in SW Taiwan, the Choshui River (63.9 × 10^6 t/yr), and the Gaoping River (35.6 × 10^6 t/yr) (Milliman and Farnsworth, 2011). These accumulated sediments provide high-resolution archives for studying environmental changes in the SE Asian continent (Li et al., 2003; Boulay et al., 2005; Liu et al., 2007a; Liu et al., 2016; Gai et al., 2020). There are many small mountainous rivers that developed in middle Vietnam (Jonell et al., 2017; Sang et al., 2018). However, unlike the small mountainous rivers in Taiwan with large amounts of sediment discharge, e.g., 54.1 Mt/yr for the Choshui River and 49.0 Mt/yr for the Kaoping River (Dadson et al., 2003), the sum of the sediment discharge in middle Vietnam is only approximately 10.0 Mt/yr (Milliman and Farnsworth, 2011). The Ba River as the largest river in middle Vietnam supplies only 1.0 Mt/yr sediments to the SCS (Milliman and Farnsworth, 2011). Early studies have suggested that their contribution to the deep-sea sediment in the SCS is almost negligible (Tan et al., 2014; Liu et al., 2016). In addition, clay mineralogy investigations on the Ba River and nearby continental shelf show that they are very rich in kaolinite and smectite, strongly different from the richness in illite and chlorite for Core MD05-2901 Holocene sediments (Liu et al., 2007b; Sang et al., 2018; Sang et al., 2019). Instead, both clay minerals and major elements in Core MD05-2901 sediments are mainly derived from end-members of the Mekong River, Red River, and Pearl River, with minor contribution from the Sunda Shelf (Liu et al., 2007a; Liu et al., 2007b; Liu et al., 2016; Sang and Liu, 2021). Therefore, we are correct to exclude the contribution of middle Vietnam to the deep-sea sediment of the SCS in later calculation. However, the enhanced anthropogenic influence of the Pearl River and the Red River in late Holocene (Hu et al., 2013; Wan et al., 2015) may need to be focused on, particularly the near-coastal regions.

The rare earth elements (REEs) are a group of trace elements whose chemical properties gradually change with their decreasing ionic radii across the lanthanide series (lanthanide contraction), from lanthanum (La) to lutetium (Lu), causing slightly different behaviors for light REEs (La–Sm, LREEs) and heavy REEs (Dy–Lu, HREEs) during dissolution, precipitation, and adsorption. These REE patterns change because of water/rock interactions, sources, or redox conditions (Toyoda et al., 1990; Nozaki, 2000; Haley et al., 2004; Wyndham et al., 2004). However, this information can be evaluated after proper standard normalization (Yusof et al., 2001) in addition to specific isotopic analyses. Owing to the strong binding capability, low natural background, and low mobility, the sediment REE patterns are considered to be essentially uniform in rocks and are not significantly affected by weathering or diagenesis (Antonina et al., 2013; Chaudhuri and Cullers, 1979; Nance and Taylor, 1977). Therefore, the REE patterns are important tracers for the investigation of sediment deposition. On the other hand, $^{87}Sr/^{86}Sr$ provide information on hydrological conditions in various chemical/physical weathering regimes (Blum and Erel, 2003; Boulay et al., 2005; Liu et al., 2011; Meyer et al., 2011), and serve as a powerful tool in global climatic change (Brass, 1976; Burke et al., 1982; Denison et al., 1998). Sr is chemically and isotopically uniform in seawater due to its long residence time, 2–2.5 Myr, compared with the ocean mixing of ~10^3 yr (Basu et al., 2001; Huang et al., 2011). ^{143}Nd is a radiogenic product of ^{147}Sm via alpha decay, half-life 1.06 × 10^{11} yr. The ε_{Nd} is not fractionated during authigenic mineral formation as well as physical/chemical weathering; thus, it can serve as a reliable provenance tracer (Goldstein and O'Nions, 1981; Li et al., 2003; Shao et al., 2009; Meyer et al., 2011). The ε_{Nd} in crust is rather heterogeneous. For example, the old granitic craton is less radiogenic, −10 to −56, compared with mantle-derived mid-oceanic ridge basalt of ~0 to +12 (Goldstein and Hemming, 2003; Jeandel et al., 2007). With this unique characteristic, ε_{Nd} is a powerful tracer for water mass identification, because the major Nd input in the ocean is from continental weathering and there is no associated isotopic fractionation during evaporation/scavenging processes (von Blanckenburg, 1999; Rutberg et al., 2000; Frank, 2002; Amakawa et al., 2004). Its oceanic residence time is ~200–1,000 yr (Elderfield et al., 1988; Tachikawa et al., 1999), shorter than the oceanic turnover time (Broecker et al., 1982). Particularly, the ε_{Nd} in the Fe-Mn oxyhydroxides can infer changes of bottom-water circulation in the past (Martin et al., 2010; Huang et al., 2014).

Three pathways of trace metal transportations to the ocean include dissolved, colloidal, and particulate, in addition to direct eolian inputs nearby dust sources. Seafloor seepages via hydrothermal vents at mid-ocean-ridge or seep sites are getting attention for the potential importance of their oceanic fluxes (Mottl et al., 2011). Frank (2002) suggested that ε_{Nd} in seawater may change with water mass mixing, external eolian dusts input, riverine particle, and shelf sediment partial dissolution. The Fe-Mn nodules, therefore, may not necessarily record sole oceanic circulation due to Nd external sources (Tachikawa et al., 2003). Any shifted ε_{Nd} values could be partially interpreted by flux changes associated with continental erosion or weathering.

In this study, we modify published leaching procedures for separation of the Fe-Mn oxyhydroxides in sediments. Subsequently, precise REEs, $^{87}Sr/^{86}Sr$, and ε_{Nd} in both the Fe-Mn oxyhydroxides and the detrital phases in 38 sliced sediments, separated from core MD05-2901 collected from the western SCS, were analyzed to evaluate controlling factors of sources, land/sea interactions, and climatic impacts over the past 32 ka. The observed co-variation of the geochemical compositions and the Sr-Nd isotopic proxies in this study supports a scenario that major sediment sources were derived from the Mekong River, the Red River, and the Pearl River, as well as the SW Taiwan rivers of the Choshui River and the Gaoping River, and the contribution of individual rivers has changed largely along with the climatic events in the past 32 ka.

2 Regional geological settings

The SCS offers an opportunity for studying fluvial sediment transportation mode among other global marginal seas (Liu et al., 2016). This region plays a critical role for chemical and heat exchange in the tropical Pacific. The high deposition rate of sedimentary cores in the SCS is capable of recording both glacial/interglacial oscillations and monsoonal climatic changes (Clift et al., 2014). The Calypso core, MD05-2901 (14°22.503'N, 110°44.6'E, 1,454 m water depth, Figure 1), is located in a summer upwelling

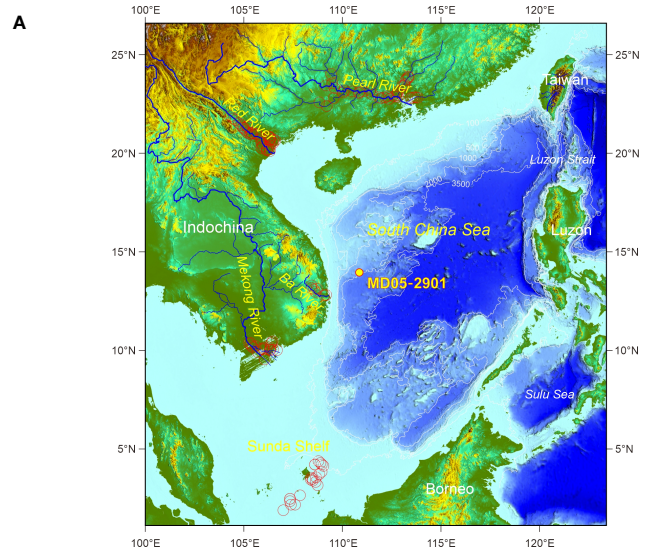

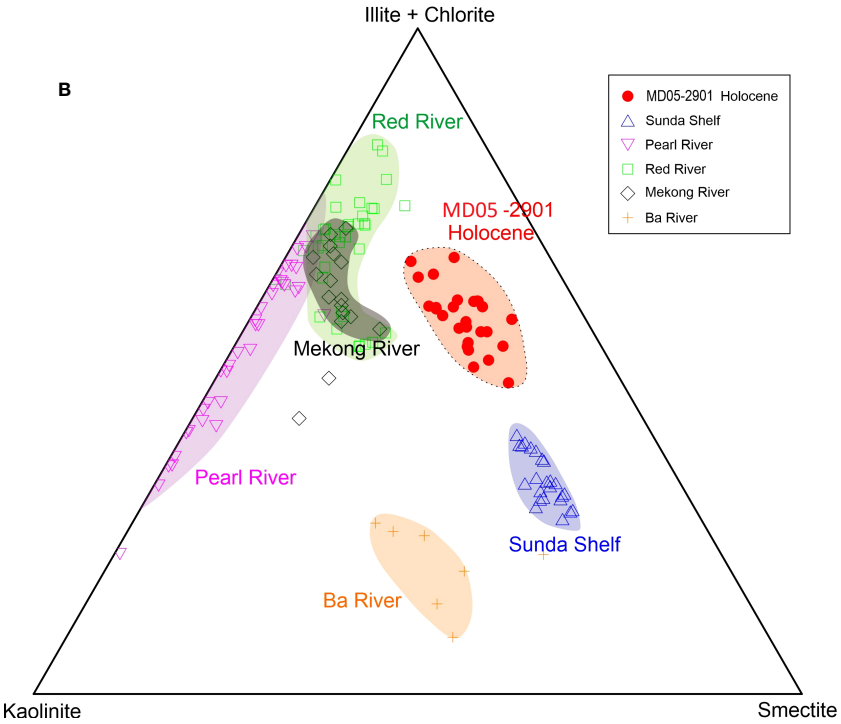

FIGURE 1
(A) A geographical map shows the study area in the northwestern SCS. The circle is the location of core MD05-2901 (14°22.50'N, 110°44.60'E), a well-dated core and provided with high-resolution climatic records. Some major rivers nearby Indochina such as the Mekong River, Red River, and Pearl River, as well as adjacent islands such as Borneo, Luzon, and Taiwan and marginal seas such as Celebes Sea, Sula Sea, and Luzon Strait are also included. **(B)**. A combined ternary diagram of the major clay mineral groups illite + chlorite, kaolinite, and smectite, showing that the clay mineral assemblage of Core MD05-2901 Holocene sediments is strongly different from that of the Ba River, the representative river in middle Vietnam. See panel **(A)** for the locations of these samples. Plots of clay mineral end-members of Mekong River, Red River, Pearl River, and Sunda Shelf sediments for Core MD01-2901 are also indicated. Data sources of clay minerals: Mekong River, Red River, and Pearl River from Liu et al. (2007a); Ba River from Sang et al. (2018); Sunda Shelf from Liu et al. (2016); and Core MD05-2901 Holocene from Liu et al. (2007b).

region off middle Vietnam, a well-dated sediment core retrieved from the NW margin in the SCS during the R/V Marion Dufresne MARCO POLO IMAGES XII Cruise (Liu et al., 2007b). The core is located off the coast of central Vietnam and in the western SCS. In addition to being very close to the central Vietnam continent, only minor terrigenous material can be deposited (Liu et al., 2007a). The location of this core is far from other important terrigenous sources, such as the Mekong River, the Red River, and the Pearl River. Therefore, it is particularly important to understand the main sources of sediments and their temporal variations in this region.

3 Materials and methods

3.1 Core description and age model

The MD05-2901 sediments consist of olive green or green gray hemipelagic mud, enriched with well-preserved calcareous and siliceous microfossils without obvious disturbance and no turbidites (Laj, 2005). A total of 38 samples at depth intervals of 186–416 cm that avoided potential bioturbation and have obtained well-dated $\delta^{18}O$ ages were selected for short-term high-resolution geochemical study. These analyses include REE patterns, $^{87}Sr/^{86}Sr$, and ε_{Nd} in both the Fe-Mn oxyhydroxides and the detrital phases of Core MD05-2901sediments (Appendix 1).

The age model in this core was established using high-resolution oxygen isotopic stratigraphy combined with the first and last occurrences of *G. ruber* at 3,337 cm/404 ka and 1,273 cm/120 ka, respectively (Liu et al., 2007b). Oxygen isotope compositions ($\delta^{18}O$) in planktonic foraminifera, *G. ruber* (white), were measured using a Finnigan MAT 252 mass spectrometer at the State Key Laboratory of Marine Geology, Tongji University. The isotopic values are expressed relative to the PDB standard with an external reproducibility of ±0.08‰.

In addition, to understand the sediment compositions in the nearby region, we have combined all literature results to form a ternary diagram of the major clay mineral groups illite + chlorite, kaolinite, and smectite, showing that the clay mineral assemblage of Core MD05-2901 Holocene sediments is plotted in Figure 1B for comparison; it is strongly different from that of the Ba River, the representative river in middle Vietnam (see Figure 1B for the locations of these samples). Plots of clay mineral end-members of Mekong River, Red River, Pearl River, and Sunda Shelf sediments for Core MD05-2901 are also indicated. The used data sources of clay minerals are as follows: Mekong River, Red River, and Pearl River from Liu et al. (2007a); Ba River from Sang et al. (2018); Sunda Shelf from Liu et al. (2016); Core MD01-2901 Holocene from Liu et al. (2007b).

3.2 Sequential leaching and digestion procedures

All sediments were treated with a sequential leaching protocol, modified from Chester and Hughes (1976). Approximately 200 mg of powder (≤63 μm) were sieved, weighted, and then soaked with Milli-Q water for 20 min to remove any residual porewater. Then, it was soaked with 30% H_2O_2 and 1 M sodium acetate (NaAc) to remove organic compounds and carbonates, respectively. Finally, the residual samples were soaked with 0.02 M hydroxylamine hydrochloride ($NH_2OH.HCl$) in 25% acetic acid (HH) solution at 25°C for 4 h to extract the Fe-Mn oxyhydroxide fractions.

After the above sequential leaching procedures, all residual materials were pre-digested using a mixture of 3 mL of 10 M HNO_3 and 2 mL of 60% HF at 100°C in a 15-mL PFA beaker for at least 24 h. It was dried once, and any residue was digested with a mixture of 0.5 mL of 7 M HNO_3 and 3.5 mL of 60% HF at 190°C in a high-pressure bomb for at least 48 h. After drying, the sample was dissolved with 10 M HCl to get rid of potential CaF_2.

3.3 Chemical separation for isotopic determination

For the isotopic analysis, Nd was purified following the method of Scher and Delaney (2010), which applied a single-stage separation column. Ln Resin (Eichrom), HDEHP [di-2ethylhexyl-orthophosphoric acid]-coated Teflon powder, 50–100 μm mesh, was used for ion exchange processes. Ln Resin was washed three times with 6 M HCl and 0.25 M HCl, and stored in 0.25 M HCl before used. Then, resin was packed and installed in a Bio-Spin column. The elution curves obtained show excellent separation of Nd from Ba and Sm, which may cause serious isobaric interference. Although Ce is not completely removed from the matrix, its potential isobaric interference effect was negligibly small (Huang et al., 2012; Huang et al., 2014). Two international reference materials, BHVO-2 and Nod P-1, were used as a standard of the detrital and the authigenic phases, respectively. In both cases, the total recovery of Nd was better than 90%.

The Sr in samples was purified, following procedures described in Liu et al. (2012). Acid-cleaned polypropylene columns, Eichrom Sr-Spec resins (50–100 mesh), were pre-washed three times using 3 M HNO_3 and Milli-Q water. International reference materials, BHVO-2 and Nod P-1, were used to evaluate the Nd recovery, and showed average recovery of better than 95%. The elution results also indicated a good removal of Rb isobaric interferences.

3.4 Elemental concentration measurements

All elemental concentrations were determined using SF-ICPMS (Element 2, Thermo Finnigan) installed in the Isotope Geochemistry Laboratory (IGL), Department of Earth Sciences, National Cheng Kung University. Similar procedures were applied for prepared international standard materials (BHVO-2 and Nod P-1), diluted threefold and analyzed for calibration curve. An introduction system, Aridus II^{TM}, was applied to enhance analytic sensitivity (>3 times), and to minimize potential oxide production ($^{238}UO/^{238}U$ ≤0.01%). Using Aridus II^{TM}, the interference of light REE (LREE) oxides on heavy REE (HREE) isotopes was found to be negligibly small (Aries et al., 2000).

3.5 Nd and Sr isotopic composition measurements

The measured $^{143}Nd/^{144}Nd$ ratios were normalized to $^{146}Nd/^{144}Nd = 0.7219$ for instrumental mass fractionation correction. International standards, La Jolla Nd and JNdi-1, were run during each analytical session. The measured $^{143}Nd/^{144}Nd$ ratios for La Jolla Nd and JNdi-1 were 0.511832 ± 0.000008 (2SD, n = 15), and 0.512094 ± 0.000007 (2SD, $n = 55$), respectively. JNdi-1 was used as the bracketing standard and run before and after every five samples (Huang et al., 2012). The La Jolla Nd standard was applied as a secondary standard to ensure proper accuracy and precision. Nd concentrations in all loadings were adjusted to ~100 ppb for monitoring stability and consistency analyses. Two other working standards, BHVO-2 and Nod P-1, were included in the analytical procedures and obtained $^{143}Nd/^{144}Nd$ ratios of 0.512989 ± 0.00003 (2SD, n = 5) and 0.512472 ± 0.00004 (2SD, n = 5), respectively. All Nd isotopic compositions were expressed as Ɛ notation:

$$\varepsilon_{Nd} = \left(\frac{^{143}Nd/^{144}Nd_{measured}}{^{143}Nd/^{144}Nd_{CHUR}} - 1 \right) \times 10^4$$

where CHUR stands for Chondritic Uniform Reservoir, and its present-day (143Nd/144Nd)CHUR is 0.512638 (Jacobsen and Wasserburg, 1980).

All measured $^{87}Sr/^{86}Sr$ ratios were normalized to $^{86}Sr/^{88}Sr = 0.1194$. Instrumental performance was monitored by duplicated analysis of SRM 987 standard (0.710248 ± 0.00002 (2SD, $n = 20$). The Sr concentrations in all samples were adjusted to ~150 ppb. Additionally, two international standards, BHVO-2 and Nod P-1, were used for any bias correction and we have obtained consistent results as the certified values of $^{87}Sr/^{86}Sr$ of 0.703471 ± 0.00002 (2SD, $n = 3$) and 0.709186 ± 0.000023 (2SD, $n = 2$), respectively.

3.6 Source apportionment of the detrital sediments

In this study, a Bayesian mixing model, MixSIAR, was employed to conduct multi-source mixing calculation for relative provenance contributions of the down-core sediments over the last 34 ka (Stock et al., 2018). The model incorporates the uncertainties of the isotopic signatures for each source, and was successfully applied to trace sources of mineral dusts in the South Pacific (Longman et al., 2022) and the source of Pb in Roman-age mining artifacts (Longman et al., 2018). Error structure and Markov Chain Monte Carlo sampling in the performed model were set as "Process+Residual" and "Long", respectively.

Four potential sediment sources that contribute to the sedimentary Sr-Nd isotope signals at our study site are the Pearl River (PR), Red River (RR), Mekong River (MR), and southwestern Taiwan River (SWTR). The end-member ranges of $^{87}Sr/^{86}Sr$ and ε_{Nd} for the delta sediments of these rivers are as follows: PR ($^{87}Sr/^{86}Sr$: 0.7301 ± 0.0019; ε_{Nd}: −11.9 ± 0.3), RR ($^{87}Sr/^{86}Sr$: 0.7253 ± 0.0018; ε_{Nd}: −11.4 ± 0.3), MR ($^{87}Sr/^{86}Sr$: 0.7212 ± 0.0008; ε_{Nd}: −10.1 ± 0.7), and SWTR ($^{87}Sr/^{86}Sr$: 0.71968 ± 0.00119; ε_{Nd}: −12.4 ± 0.3) (Liu et al., 2007a), which are within the isotopic ranges of delta sediments recently compiled by Duan et al. (2023). The MixSIAR mixing model was then run by the following equations for calculating relative contributions for the four sources:

$$X_M = f_{PR}X_{PR} + f_{RR}X_{RR} + f_{MR}X_{MR} + f_{SWTR}X_{SWTR}$$

$$1 = f_{PR} + f_{RR} + f_{MR} + f_{SWTR}$$

where f and X indicate the fraction and the isotopic composition, respectively. The subscript "M" denotes the measured signal for the mixture of the four sources.

4 Results and discussion

All isotopic compositions of Sr and Nd in the detrital and authigenic phases obtained are summarized in the Supplementary Table 1. Post-Archean Australian Shale (PAAS)-normalized Ce anomalies for the detrital fraction and the Fe-Mn oxyhydroxides are listed in Supplementary Tables 1, 2, respectively. It is critical to select a proper reference for REE normalization purposes (Nozaki, 2000), where PAAS represents average REEs in the upper continental crust and the shale-normalized REEs can be used to visualize fractionation derived from different continental sources (Taylor and McLennan, 1985; McLennan, 1989; Pourmand et al., 2012). The PAAS-normalized REE patterns for the authigenic and detrital fractions at different depths in MD05-2901 sediments are plotted in Figure 2. The REEs in the detrital fractions display a relatively flat pattern, average $(La/Yb)_{PAAS} = 0.911$, average $(La/Gd)_{PAAS} = 0.863$, and slight positive Ce anomaly $Ce/Ce^*_{average} = 1.1$ (Supplementary Table 1), implying similar REEs to the typical continental shale. The REEs in the authigenic phase display middle REE (MREE) enrichment [average $(Gd/La)_{PAAS} = 2.7$] and slightly high heavy REE (HREE) [average $(Yb/La)_{PAAS} = 1.28$]. The calculated Ce/Ce* ratio varies from 1.63 to 1.72, indicating a strong positive Ce anomaly in REEs. On the other hand, the detritus fractions show rather flat patterns with a small Ce anomaly (Figure 2). The detrital fractions in the SCS sediments are mainly aluminosilicates, almost no carbonate. Thus, the carbonate removed using the leaching methods is authigenic and marine carbonate. Then, the removal of REEs of carbonate will not affect the composition of REEs in detrital fractions.

The measured Sr and $^{87}Sr/^{86}Sr$ as well as other parameters derived from mass balance calculations are summarized in Supplementary Table 3. The Fe-Mn oxyhydroxide fractions contain 1.6–2.5 μg/g Sr, and $^{87}Sr/^{86}Sr$ varied in a narrow range, 0.709262–0.709313, during the last 32 ka. The $^{87}Sr/^{86}Sr$ in Fe-Mn oxyhydroxides are significantly higher than the average seawater (~0.7092) in the Pleistocene–Holocene (Figure 3A), but much lower than the associated terrigenous detritus fractions (0.7232–0.7265); similar discordance was reported by Gutjahr et al. (2007).

The ε_{Nd} records of the detrital and the authigenic phases in MD05-2901 sediments over the last 32 ka were compiled in

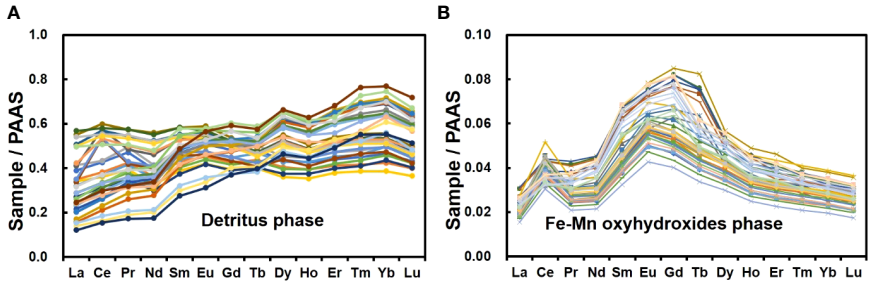

FIGURE 2
PAAS-normalized REE patterns for **(A)** the detritus fractions and **(B)** the Fe-Mn oxyhydroxide fractions, and HH-extractions at different depths of MD05-2901 sediments. Symbols: diamonds: detritus; squares: authigenic.

Figure 3B. During the period of 8.5–32 ka, the ε_{Nd} values in the detrital fractions, residual after HH procedures, vary between −12.5 and −10.3; average = −11.4. The ε_{Nd} values of both the detrital and the authigenic fractions are relatively stable (−11.2 or −8.0) during 32–23 ka. However, a sharp increased ε_{Nd}, up to −10.3, was observed at early Last Glacial Maximum (LGM, 23–19 ka) and during Younger Dryas (YD, ~13–11.5 ka). In contrast, the ε_{Nd} is low (−12.1) during the Heinrich 1 event (H1, 17.5–15 ka). Most of these ε_{Nd} values display a strong correlation with the environmental changes/climatic events. These results display a similar trend within ~2ε variations in both fractions. The overall ε_{Nd} is more radiogenic during the cold periods (e.g., YD and LGM) and shows less radiogenic values during the warm period (e.g., the Bølling/Allerød, B/A). The average ε_{Nd} value in the detritus and the authigenic phase is −11.4 and −7.7, respectively.

Additional correlation plots among LREE, HREE, MREE/MREE*, $^{87}Sr/^{86}Sr$, and ε_{Nd} in the authigenic fractions are shown in Supplementary Figure 1, where there is no significant correlation

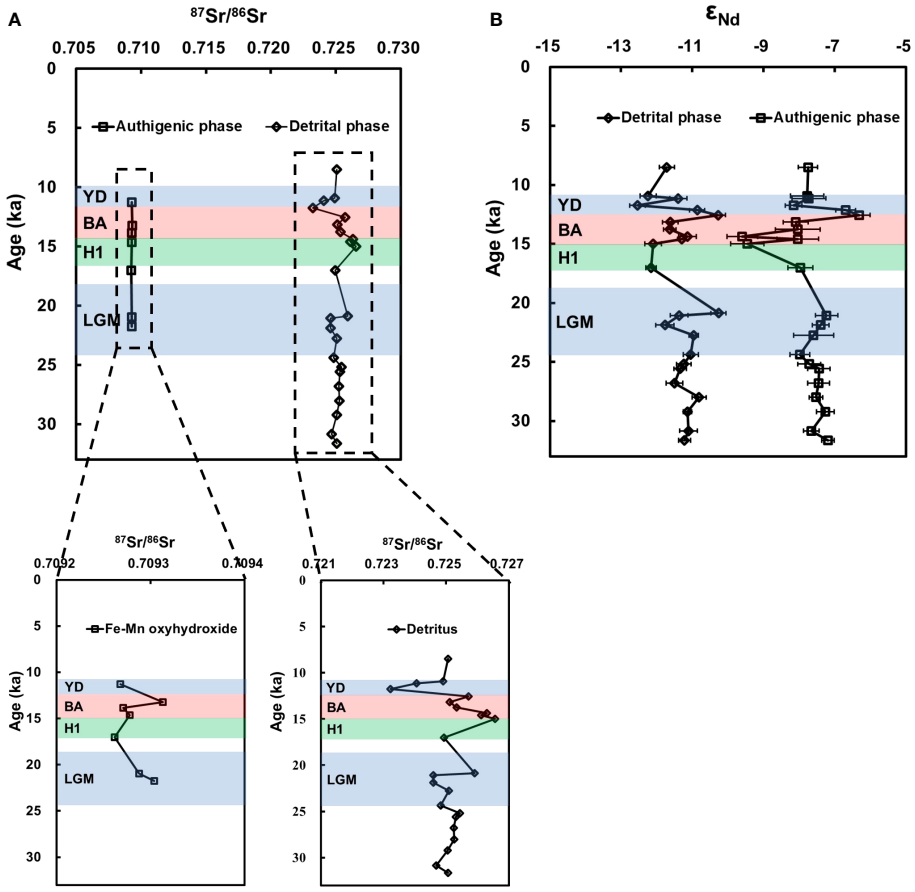

FIGURE 3
Temporal plots of $^{87}Sr/^{86}Sr$ **(A)** and ε_{Nd} **(B)** variations in the Fe-Mn oxyhydroxides and the detrital phases of core MD05-2901 sediments over the last 32 ka. The box regions in **(A)** were zoomed in below for clear visibility purposes.

for the authigenic fractions, except the ε_{Nd} vs HREE plot shown in (b). In addition, HREE/LREE = (Tm+Yb+Lu)/(La+Pr+Nd) and MREE/MREE* = (Gd+Ty+Db)/[(Tm+Yb+Lu+La+Pr+Nd)/2] are defined, respectively. The data points deviated from the main trend of low ε_{Nd}, with more abundant HREEs being consistent with the addition of river sediments from southwestern Taiwan in the Holocene and YD (Li et al., 2013).

4.1 REE patterns

The average PAAS-normalized REE patterns in the detrital fractions of the MD05-2901 sediments are rather flat, indicating similar REE pattern compositions to the upper continental crust. The MREE-enriched patterns in the Fe-Mn oxyhydroxides have been attributed to selective adsorption/incorporation of MREE (Haley et al., 2004; Gutjahr et al., 2007), probably generated by oxidation of Ce^{3+} to insoluble Ce^{4+} during the formation (Haley et al., 2004; Wyndham et al., 2004; Huang et al., 2014) and agrees with the assumption of bottom disturbance to enhance Ce^{3+} transferred from interstitial water (Alibo and Nozaki, 2000). Martin et al. (2010) presented robust procedures to evaluate if the water mass signature can be extracted from sediments using the HH-leaching method. A cross-plot of HREE/LREE and MREE/MREE* displays three typical groups (Figure 4): (1) 1.5< MREE/MREE*< 2 and 0.9< HREE/LREE< 1.3 in HH-extractions and Fe-Mn nodules (e.g., Nod P-1 standard); (2) 0.9< MREE/MREE*< 1.1 and 0.9< HREE/LREE< 1.4 in the detrital phase of MD05-2901 sediments; (3) 0.9< MREE/MREE*< 1.3 and 3.6< HREE/LREE< 4.3 in various seawaters collected from North Atlantic, South India, and the SCS, where HREE/LREE = (Tm+Yb+Lu)/(La+Pr+Nd) and MREE/MREE* = (Gd+Ty+Db)/[(Tm+Yb+Lu+La+Pr+Nd)/2] (Martin et al., 2010). Our results clearly show that the Fe-Mn oxyhydroxides can be separated from the detritus. These results strongly support the sequential leaching steps that effectively separated two phases in sediments if the boundary scavenging effects can be evaluated separately. Our preliminary results in Figure 2 further demonstrate small REE pattern variations in the SCS seawater over the last 32 ka.

4.2 Sr isotopic mixing

Bayon et al. (2002) found high $^{87}Sr/^{86}Sr$ (~0.7093), but similar deep seawater ε_{Nd} in leachate in the youngest MD96-2086 sediments. Later, Piotrowski et al. (2004) proposed that $^{87}Sr/^{86}Sr$ in the Fe-Mn oxyhydroxides phase is a sensitive proxy for detritus contamination, because a large isotopic difference existed in the two phases. Even a small detrital Sr involved would cause a significant offset in the sequential leaching results. In addition, boundary exchange may complicate the issue as it may have occurred during the Fe-Mn oxyhydroxide formation. To examine possible detritus contamination, the measured Sr and $^{87}Sr/^{86}Sr$ in the Fe-Mn oxyhydroxides and the detrital fractions were utilized to perform a simple mass balance calculation. As Nd is highly enriched in the Fe-Mn oxyhydroxides, it is less prone to disturbance (Gutjahr et al., 2007). The detritus contribution (f) associated with the Fe–Mn oxyhydroxides in MD05-2901 sediments is estimated by assuming a present-day seawater $^{87}Sr/^{86}Sr$ of 0.70918 (Henderson et al., 1994). We found that the f values vary only 0.5%–0.8% (Supplementary Table 3). The total detritus Sr in the Fe-Mn oxyhydroxides, $[Sr]_{detri.authi}$, can then be estimated, as well as the Sr leached (p) from the detritus (Supplementary Table 3).

The preliminary calculations based on the determined Sr isotopic compositions are listed in Supplementary Table 3, where p represents the total amount of leached detrital Sr (%); $[Sr]_{detri.authi}$ is the leached detritus presented in the authigenic fraction and $[Sr]_{detrital}$ is the Sr in the detritus fractions. The average p is ~0.02% in this core and provides useful information on detritus contamination. The Sr isotopic compositions in respective fractions, as well as the imprinted detritus contamination, can be estimated if seawater Sr is assumed. Our results suggest that the

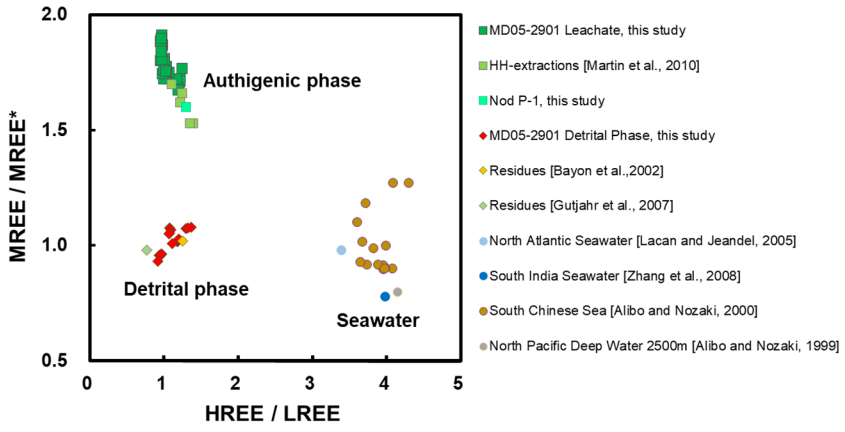

FIGURE 4
The comparison plots of PAAS-normalized HREE/LREE vs. MREE/MREE* for the HH-extraction, residues, and seawater in the South China Sea. Literature data including seawater from various oceans and sediment extractions and residuals (Bayon et al., 2002; Lacan and Jeandel, 2005; Gutjahr et al., 2007; Martin et al., 2010; Zhang et al., 2008; Alibo and Nozaki, 1999; Alibo and Nozaki, 2000). Symbols: diamonds: detritus; squares: authigenic.

$^{87}Sr/^{86}Sr$ in the Fe-Mn oxyhydroxides have carried imprints from the detritus contamination, partially due to boundary exchange. This leads to the observed $^{87}Sr/^{86}Sr$ variations in authigenic fractions, 0.709262–0.709313 (Supplementary Table 3).

4.3 Nd isotopic signature

The co-variation in Nd isotopic compositions between the detritus and the Fe-Mn oxyhydroxide phases can be explained by either coincidence local events or boundary exchange processes. The former suggests that possible events may have occurred related to sediment source or weathering region. The latter supports the ε_{Nd} distributions controlled by boundary exchange processes occurring at the continental/ocean interface.

The oceanic Nd budget, with consistent dissolved Nd fluxes into the ocean, was calculated in Tachikawa et al. (2003), assuming that partial Nd fluxes have exchanged between the dissolved ones and the particulates in sediments. The Nd flux estimated is 9×10^9 g/yr entering the ocean, yielding an oceanic Nd residence time of ~500 yr. Nd sources to the ocean may vary from region to region, where riverine and atmospheric eolian fluxes cannot explain the observed variability. Additional missing sources of Nd must be considered to balance the oceanic budget.

The particle exchange of Nd may have occurred in various areas, depending on lithology, water depth, climate, weathering regime, intensity of primary productivity, and hydrodynamics. These processes could have an importance similar to or greater than that of net terrigenous inputs into marine sediments globally and could be enhanced under high hydrodynamic conditions (Lacan and Jeandel, 2005). The study core MD05-2901 is located in the summer upwelling region offshore central Vietnam (Liu et al., 2007b). The ε_{Nd} values show significant modification of the Fe-Mn oxyhydroxide signatures recorded in the sediments due to the particle exchange or modern seawater pollution. The high $^{87}Sr/^{86}Sr$ ratios in the Fe-Mn oxyhydroxides phases, as well as the calculation of Sr mass balance results, support the former hypothesis of potential particle exchange (Lacan and Jeandel, 2005) that may have occurred at this site.

4.4 Abrupt climatic changes

Abrupt climatic events may affect the ε_{Nd} distribution in the authigenic phase. Significant changes in Nd isotope were reported in fish teeth from a core located in Baja California (Basak et al., 2010). The abrupt cooling of H1 believed to be caused by melting waters inflow at high latitude, such as the Laurentide Ice Sheet, and thermohaline circulation was slowed down or even shut down during H1 (McManus et al., 2004). More independent data are needed to pin down controlling mechanisms of sedimentary Nd in the shelf regions.

At the location of MD05-2901, large fluxes of particles may have imported from the continent and acted as effective media to scavenge dissolved elements along the land/sea interface, which could enhance the effect of boundary exchange at the study site. Based on the above-mentioned discussion, we propose that particle exchange has been intensively involved in the studied site over the last 32 ka, and our authigenic Nd isotope record can serve as a probe for continental/sediment input in the SCS.

4.5 Sediment provenance of Core MD05-2901

The Sr and Nd isotopic compositions in the detritus can be used as source fingerprint of sediments. During the period of 8.5–32 ka, the $^{87}Sr/^{86}Sr$ ratio in the detritus falls in a range of 0.72322–0.72656, with an average of 0.72515 (Figure 3A). There is no significant Sr isotopic composition change observed at the LGM or H1. A maximum $^{87}Sr/^{86}Sr$ ratio, 0.72656, was observed at the onset of B/A, 14.5–13 ka. The ratio tends to decrease through time after B/A, and reach a minimum, 0.72322, at YD. In the Holocene, the average value is ~0.72520, approximately the same as the average of the entire study period. It is believed that more enhanced chemical weathering was prevailing during a warm period, such as B/A.

The majority of seafloor sediments were derived from eolian dust and adjacent large river inputs. In particular, thick piles of riverine sediments accumulated in the northern and western SCS (Li et al., 2003; Boulay et al., 2005; Yang and Youn, 2007). Some previous studies did not include dusts as elemental sources in the northern and western SCS (Liu et al., 2003; Boulay et al., 2005; Liu et al., 2007a). Assuming an aerosol flux equal to or less than the modern value, 0.5 g cm^{-2} ka^{-1}, dusts may account for ~5% terrigenous flux at most sites in the northern and western SCS (Duce et al., 1991). For this reason, we assumed that the dusts from Gobi and Junggar Basin would not be a major source in the following discussion.

Three major rivers (i.e., the Pearl, Red, and Mekong River) are adjacent to the MD05-2901 in the western SCS. Sediments from southwestern Taiwan were considered to be a minor source based on clay minerals (Liu et al., 2007a). Although Taiwan provides a large amount of sediments to the ocean (approximately 400×10^6 t/yr), only ~150×10^6 t/yr can reach the SCS (Dadson et al., 2003; Boulay et al., 2005). Moreover, based on a clay distribution study, it was proposed that the main sediment sources of the northern and western SCS were within the adjacent basins (Liu et al., 2007a). All these arguments are consistent with our MixSIAR modeling calculations (mean ± SD) (RR: 46% ± 20%, PR: 25% ± 10%, MR: 17% ± 7% and SWTW: 12% ± 4%) for the sediment samples used in this study.

The Mekong River sediments display a rather narrow range in $^{87}Sr/^{86}Sr$ (0.720–0.722) and ε_{Nd} (−9.9 to −10.8). The Pearl and Red River have similar range of ε_{Nd} (−10.4 to −13.3), but different $^{87}Sr/^{86}Sr$, in a range of 0.728–0.742 and 0.716–0.734, respectively. Liu et al. (2007a) studied the clay distribution in SCS and found that clay minerals are sensitive to the types of environmental conditions clays produced, with more physical erosion in the Red and the Mekong River basins than that in the Pearl River (Liu et al., 2007a).

Modern bulk river sediments show relatively low ε_{Nd} (−12 to −15) and wide $^{87}Sr/^{86}Sr$ (0.720–0.730) in southern Taiwan (Chen et al., 1990). Our $^{87}Sr/^{86}Sr$ results reach similar conclusions, indicating more intense chemical weathering in the Pearl River, compared with those of the Red River and the Mekong River.

The $^{87}Sr/^{86}Sr$ and ε_{Nd} were plotted in Figures 5A, B, which show a small range of distributions in MD05-2901 sediments, compared with available literature data in the Luzon basalt, East and SW Taiwan, and the Pearl, the Red, and the Mekong River regions. These results suggest limited changes in sediment sources at our study site over the past 32 ka. Moreover, the Red River and the Mekong River showed low $^{87}Sr/^{86}Sr$, possibly indicating either high physical erosion condition or more intense carbonate weathering. On the other hand, the Pearl River data support a source region with enhanced chemical weathering.

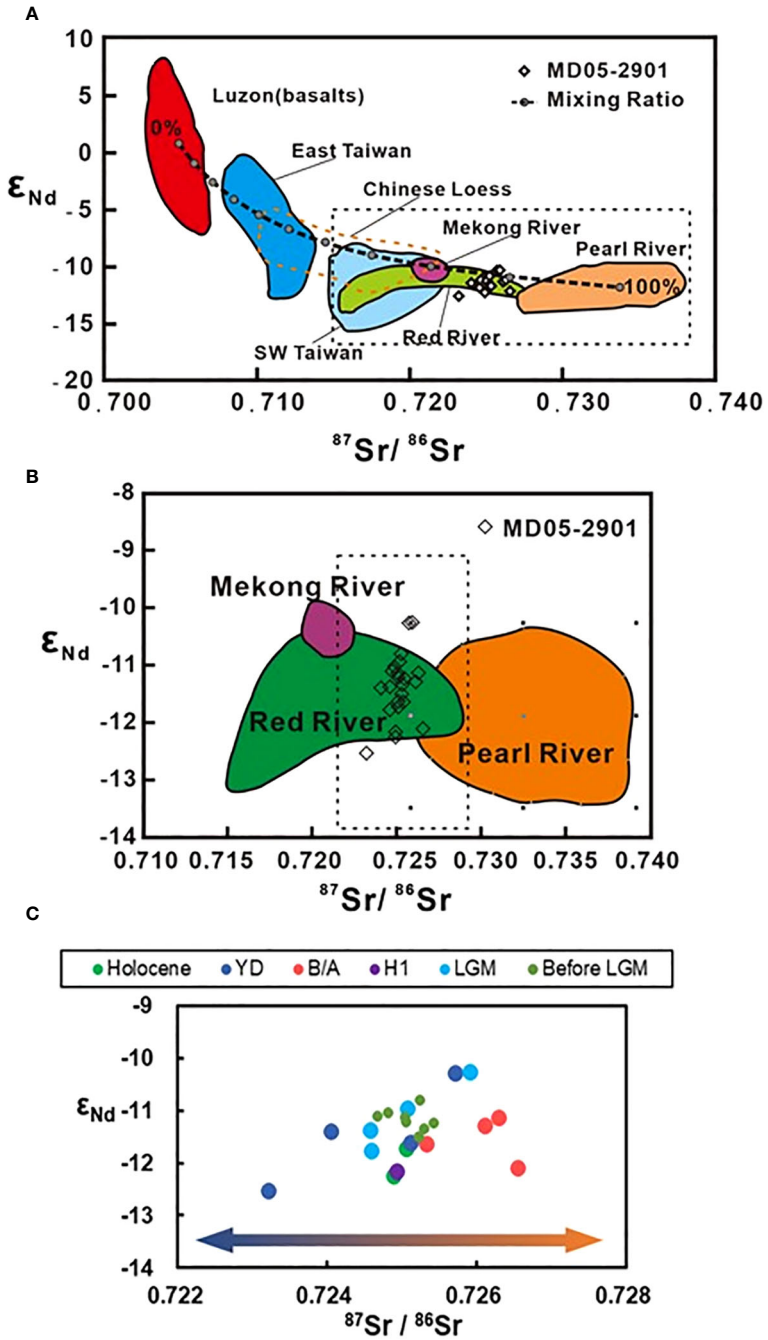

FIGURE 5
The sediment mixing plots of **(A)** a crossed plot of $^{87}Sr/^{86}Sr$ and ϵ_{Nd} in the detritus fraction (diamonds). Circles represent the end-member proportion of Pearl River-derived components with 10% intervals, assuming only two major end-members mixing among Luzon Arc, Pearl River, and modern SW Taiwan sediments (for data sources of ε_{Nd}-$^{87}Sr/^{86}Sr$, see Supplementary Table 1; Chen et al., 1990; Liu et al., 2007a); inserted dashed square box shows the zoomed-in range in **(B)**. **(B)** A cross-plot of ε_{Nd} values and $^{87}Sr/^{86}Sr$ ratios for the detrital fraction, as well as the distribution of the three major rivers; inserted dashed square box shows the zoomed-in range in **(C)**. **(C)** A cross-plot of ε_{Nd}-$^{87}Sr/^{86}Sr$ in the detritus fraction. The isotopic ranges of three potential sources, Mekong, Red, and Pearl River, are shown by the dashed line; $^{87}Sr/^{86}Sr$ and ε_{Nd} data are quoted from Liu et al. (2007a).

The similarity of the Nd isotopic variations between authigenic and detrital fractions has suggested that chemical signatures of authigenic phases are, to some extent, influenced by the detrital phases. We think that this is also the reason why the reconstructed Nd/Sr isotopic records were considered as an indicator for particle exchange, not for the seawater signals in this study. A slightly positive Ce anomaly (oceanic ferromanganese encrustation and nodules are also typically characterized by a pronounced positive Ce anomaly, Elderfield et al., 1981) in the authigenic phases observed in the SCS sediments likely reflects elevated dissolved Ce concentrations at around 2,000 m water depth (near the sill depth) in the SCS (Alibo and Nozaki, 2000). These authors attribute this anomaly of high dissolved Ce concentration around the sill depth to the release of Ce (III) (formed by a diagenetic process in the marine sediments under sub-anoxic conditions) from the interstitial water due to the disturbance of the sediments by strong bottom currents in the Luzon Strait.

4.6 Climatic control on sediment provenance

The Sr and Nd isotopic results in detritus obtained suggest insignificant source region variation in the sediments of MD05-2901 over the last 32 ka. However, subtle changes in detrital Nd and Sr isotopic compositions were observed in coincidence with abrupt climatic events. In general, ε_{Nd} values vary inversely to those of the Sr isotopes, with less radiogenic $^{87}Sr/^{86}Sr$ associated with more radiogenic ε_{Nd} during the YD period. These data were subdivided into six climatic intervals for discussion: Holocene, YD (13–11.5 ka), B/A (14.5–13 ka), H1 (17.5–15 ka), the LGM (23–19 ka), and before the LGM (Figure 5C). In order to evaluate the source contributions through time, the MixSIAR model was applied for multi-variate mixing calculation. Although the uncertainty (~40% of the mean value) for the contributions from each source was relatively large compared to the overall variations, the model results provide useful information about changes in sediment provenance during the climatic intervals. The uncertainty may be significantly reduced by better constraints on the source compositions.

There are several YD and B/A data points that clearly deviated from the average values of $^{87}Sr/^{86}Sr$ (0.71459–0.72544) and ε_{Nd} (−12.2 to −10.8). The shifted isotopic compositions detected in the YD are probably caused by increased sediment contributions from the Mekong River (17% ± 1% before YD vs. 21% during YD) and Taiwan rivers (13% ± 1% before YD vs. 17% during YD) based on the MixSIAR model outputs (Figure 6). In contrast, the high $^{87}Sr/^{86}Sr$ during the B/A may indicate increased inputs of the Red River and Pearl River sediments. It is evident that abrupt climatic changes sensitively affect the sediment provenances in the MD05-2901. In the cold periods, accelerated aridity enhances physical erosion, in contrast to that of increased monsoon rainfall, characterized by strong chemical weathering over the continent during warm periods (Boulay et al., 2005).

All available geochemical results in MD05-2901 obtained in this study are summarized in the age profile figure, including $^{87}Sr/^{86}Sr$ and ε_{Nd} of the Fe-Mn oxyhydroxides and the detrital phases, as well as $\delta^{18}O$ in foraminiferal shells (Liu et al., 2007b) to compare with the ice core NGRIP $\delta^{18}O$ (Vinther et al., 2006). It should be noted that we have no specimens younger than 8.51 ka in this study and that there is a lack of precise dates due to potential bioturbation mixing. Therefore, the arguments of anthropogenic impacts in late Holocene is beyond the scope of this study (Hu et al., 2013; Wan et al., 2015). The narrow $^{87}Sr/^{86}Sr$ variations in MD05-2901 imply that an insignificant source changed in the past 32 ka. Moreover, the detectable $^{87}Sr/^{86}Sr$ variations found in the YD, B/A, and the LGM imply that the contributions of Red and the Mekong Rivers may have increased during YD and the LGM. In contrast, the Red River and Pearl River components have increased during the warm period in B/A. These results suggest that abrupt climatic changes can lead to shifts in weathering regions and affect the riverine sources in the SCS sediments (Figure 7). Although the sediment provenances may not be changed significantly, the sediment contributions of different sources varied over the last 32 ka according to the calculation present in this study.

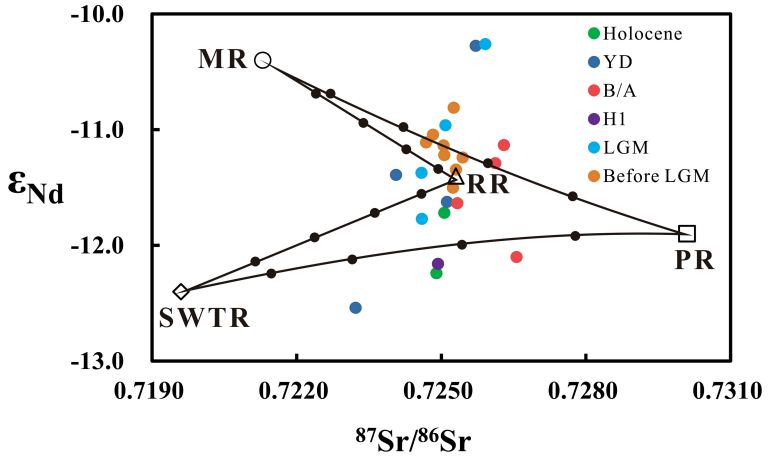

FIGURE 6
A cross-plot of $^{87}Sr/^{86}Sr$-ε_{Nd} in the detritus fractions, as well as estimated distribution of major rivers in the study region. Black circle represents the proportion of each component; symbols: Mekong (circle), Red (triangle), Pearl River (square), and SW Taiwan (diamond), of 20% interval.

10.3389/fmars.2023.1292802

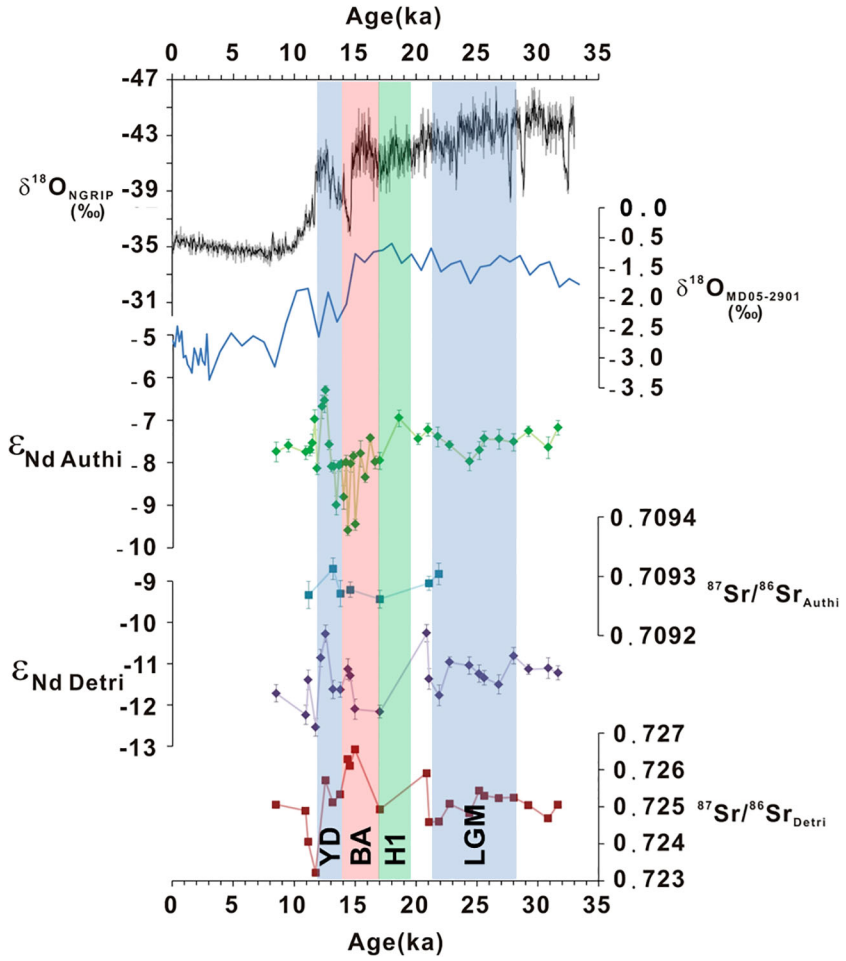

FIGURE 7
The integrated age profiles of $^{87}Sr/^{86}Sr$, ε_{Nd} in the Fe-Mn oxyhydroxides and the detritus phase in the core MD05-2901, compared with the $\delta^{18}O_{NGRIP}$ in Greenland ice core and $\delta^{18}O_{foram}$ in MD05-2901 over the last 32 ka. The $\delta^{18}O$ results were quoted from ice core and foraminiferal shells in SCS [see Vinther et al. (2006) and Liu et al. (2007b), respectively]. The error bar of each data point is smaller than the size of the symbols presented. Please note that the youngest sediments were 8.51 ka and any potential anthropogenic impacts in late Holocene cannot be considered in this study.

5 Conclusions

We have studied REEs, Sr, and Nd isotopic compositions in the authigenic Fe-Mn oxyhydroxides and the detrital fractions in MD05-2901 sediments in the SCS. The systematic ε_{Nd} differences between the detritus and the Fe-Mn oxyhydroxide phases allowed us to examine issues related to the particle exchange in the ocean.

Moreover, high $^{87}Sr/^{86}Sr$ values (~0.7093) in the authigenic phase indicate potential Sr exchanges with the detritus in sediments. It is evident that particle exchange plays an important role in mass balance in the SCS over the past 32 ka.

There are potential end-members in MD05-2901 sediments based on $^{87}Sr/^{86}Sr$ and ε_{Nd}, namely, the Pearl River, the Red River, the Mekong River, and rivers in SW Taiwan. The riverine sediments can account for 90% of sediments that accumulated at the study site. However, some of the detrital Sr and Nd isotopes at different time episodes fall outside the mixing trends among the Mekong River, the Red River, the Pearl River, and the SW Taiwan rivers, and need more in-depth investigation in the future; in addition, the potential anthropogenic impacts on continental weathering and near-coastal sediments in late Holocene, younger than 8.51 ka, need to be further explored, such as the Jonell et al. (2017) study in central Vietnam. This study is limited by the sampling resolution in this core and its lack of the uppermost recent sediments.

Data availability statement

The original contributions presented in the study are included in the article/Supplementary Material. Further inquiries can be directed to the corresponding author.

Author contributions

C-FY: Conceptualization, Data curation, Funding acquisition, Methodology, Project administration, Resources, Supervision, Validation, Writing – original draft, Writing – review & editing. W-LL: Data curation, Formal analysis, Methodology, Writing – original draft, Writing – review & editing. K-FH: Data curation,

Software, Writing – review & editing. C-HC: Conceptualization, Data curation, Formal analysis, Methodology, Validation, Writing – review & editing. ZL: Data curation, Investigation, Software, Validation, Writing – review & editing.

Funding

The author(s) declare financial support was received for the research, authorship, and/or publication of this article. The study was support by National Science and Technology Council, Taiwan (grant number 112-2116-M-006-008).

Acknowledgments

We thank all cruise members on board R/V Marion Dufresne cruise IMAGES-MARCO POLO for the collection of core MD05-2901 sediments. The constructive suggestions by the reviewers in the early draft manuscript has improved this manuscript.

Conflict of interest

The authors declare that the research was conducted in the absence of any commercial or financial relationships that could be construed as a potential conflict of interest.

Publisher's note

Supplementary material

The Supplementary Material for this article can be found online at: https://www.frontiersin.org/articles/10.3389/fmars.2023.1292802/full#supplementary-material

References

Alibo, D. S., and Nozaki, Y. (1999). Rare earth elements in seawater: particle association, shale-normalization, and ce oxidation. *Geochim. Cosmochim. Acta* 63, 363–372. doi: 10.1016/S0016-7037(98)00279-8

Alibo, D. S., and Nozaki, Y. (2000). Dissolved rare earth elements in the South China Sea: Geochemical characterization of the water masses. *J. OF GEOPHYS. Res.* 105, 28771–28783. doi: 10.1029/1999JC000283

Amakawa, H., Nozaki, Y., Alibo, D. S., Zhang, J., Fukugawa, K., and Nagai, H. (2004). Neodymium isotopic variations in Northwest Pacific waters. *Geochimica Cosmochimica Acta* 68, 715–727. doi: 10.1016/S0016-7037(03)00501-5

Antonina, A. N., Shazili, N. A. M., Kamaruzzaman, B. Y., Ong, M. C., Rosnan, Y., Sharifah, F. N., et al. (2013). Geochemistry of the rare earth elements (REE) distribution in terengganu coastal waters: A study case from redang island marine sediment. *Open J. Mar. Sci.* 3, 154–159. doi: 10.4236/OJMS.2013.33017

Aries, S., Valladon, M., Polvé, M., and Dupré, B. (2000). A routine method for oxide and hydroxide interference corrections in ICP-MS chemical analysis of environmental and geological samples. *Geostandards Newslett.* 25, 19–31. doi: 10.1111/j.1751-908X.2000.tb00583.x

Basak, C., Martin, E. E., Horikawa1, K., and Marchitto, T. M. (2010). Southern Ocean source of ^{14}C-depleted carbon inthe North PacificOcean duringthe last deglaciation. *Nat. Geosci.* 3, 770–773. doi: 10.1038/ngeo987

Basu, A. R., Jacobsen, S. B., Poreda, R. J., Dowling, C. B., and Aggarwal, P. K. (2001). Large groundwater strontium flux to the oceans from the bengal basin and the marine strontium isotope record. *Science* 293, 1470–1473. doi: 10.1126/science.1060524

Bayon, G., German, C. R., Boella, R. M., Milto, J. A., Taylor, R. N., and Nesbitt, R. W. (2002). An improved method for extracting marine sediment fractions and its application to Sr and Nd isotopic analysis. *Chem. Geol.* 187, 179–199. doi: 10.1016/S0009-2541(01)00416-8

Blum, J. D., and Erel, Y. (2003). "5.12 - Radiogenic Isotopes in Weathering and Hydrology, In: Editors-in-Chief," in *Treatise on Geochemistry*. Eds. D. H. Heinrich and K. T. Karl (Pergamon, Oxford: Elsevier), 365–392.

Boulay, S., Colin, C., Trentesaux, A., Frank, N., and Liu, Z. (2005). Sediment sources and East Asian monsoon intensity over the last 450 ky. Mineralogical and geochemical investigations on South China Sea sediments. *Palaeogeogr. Palaeoclimatol. Palaeoecol.* 228, 260–277. doi: 10.1016/j.palaeo.2005.06.005

Brass, G. W. (1976). The variation of the marine ^{87}Sr/^{86}Sr ratio during Phanerozonic time: interpretation using a flux model. *Geochimica Cosmochimica Acta* 40, 721–730. doi: 10.1016/0016-7037(76)90025-9

Broecker, W. S., Peng, T., Beng, Z., and Observatory, L.-D. G. (1982). *Tracers in the sea* (Columbia University: Lamont-Doherty Geological Observatory).

Burke, W. H., Denison, R. E., Hetherington, E. A., Koepnick, R. B., Nelson, H. F., and Otto, J. B. (1982). Variation of seawater ^{87}Sr/^{86}Sr throughout Phanerozoic time. *Geology* 10, 516–519. doi: 10.1130/0091-7613(1982)10<516:VOSSTP>2.0.CO;2

Chaudhuri, S., and Cullers, R. L. (1979). The distribution of rare-earth elements in deeply buried gulf coast sediments. *Chem. Geol.* 24, 327–338. doi: 10.1016/0009-2541(79)90131-1

Chen, C. H., Jahn, B. M., Lee, T., Chen, C. H., and Cornichet, J. (1990). Sm-Nd isotopic geochemistry of sediments from Taiwan and implications for the tectonic evolution of southeast China. *Chem. Geol.* 88, 317–332. doi: 10.1016/0009-2541(90)90096-P

Chester, R., and Hughes, M. J. (1976). A chemical technique for the separation of ferro-manganese minerals, carbonate minerals and adsorbed trace elements from pelagic sediments. *Chem. Geol.* 2, 249–262. doi: 10.1016/0009-2541(67)90025-3

Clift, P. D., Wan, S., and Blusztajn, J. (2014). Reconstructing chemical weathering, physical erosion and monsoon intensity since 25 Ma in the northern South China Sea: A review of competing proxies. *Earth-Science Rev.* 130, 86–102. doi: 10.1016/j.earscirev.2014.01.002

Dadson, S. J., Hovius, N., Chen, H., Dade, W. B., Hsieh, M.-L., Willett, S. D., et al. (2003). Links between erosion, runoff variability and seismicity in the Taiwan orogen. *Nature* 426, 648–651. doi: 10.1038/nature02150

Denison, R. E., Koepnick, R. B., Burke, W. H., and Hetherington, E. A. (1998). Construction of the Cambrian and Ordovician seawater ^{87}Sr/^{86}Sr curve. *Chem. Geol.* 152, 325–340. doi: 10.1016/S0009-2541(98)00119-3

Duce, R. A., Liss, P. S., Merrill, J. T., Atlas, E. L., Buat-Menard, P., Hicks, B. B., et al. (1991). The atmospheric input of trace species to the world ocean. *Global Biogeochem. Cycles* 5, 193–259. doi: 10.1029/91GB01778

Elderfield, H., Whitfield, M., Burton, J. D., Bacon, M. P., and Liss, P. S. (1988). "The Oceanic Chemistry of the Rare-Earth Elements [and Discussion]," in *Philosophical Transactions of the Royal Society of London. Series A, Mathematical and Physical Sciences*. (London: The Royal Society Publisher), vol. 325, 105–126.

Elderfield, H., Hawkesworth, C. J., Greaves, M. J., and Calvert, S. E. (1981). Rare earth element geochemistry of oceanic ferromanganese nodules and associated sediments. *Geochim. Cosmochim. Acta* 45, 513–528. doi: 10.1016/0016-7037(81)90184-8

Frank, M. (2002). Radiogenic isotopes: Tracers of past ocean circulation and erosional input. *Rev. Geophys.* 40, 1–38. doi: 10.1029/2000RG000094

Gai, C., Liu, Q., Roberts, A. P., Chou, Y., Zhao, X., Jiang, Z., et al. (2020). East Asian monsoon evolution since the late Miocene from the South China Sea. *Earth Planet. Sci. Lett.* 530, 115960. doi: 10.1016/j.epsl.2019.115960

Goldstein, S. L., and Hemming, S. R. (2003). Long-lived isotopic tracers in oceanography, paleoceanography, and ice-sheet dynamics, treatise on geochemistry. *Elsevier*, 453–489. doi: 10.1016/B978-0-08-095975-7.00617-3

Goldstein, S. L., and O'Nions, R. K. (1981). Nd and Sr isotopic relationships in pelagic clays and ferromanganese deposits. *Nature* 292, 324–327. doi: 10.1038/292324a0

Gutjahr, M., Frank, M., Stirling, C., Klemm, V., Vandeflierdt, T., and Halliday, A. (2007). Reliable extraction of a deepwater trace metal isotope signal from Fe–Mn oxyhydroxide coatings of marine sediments. *Chem. Geol.* 242, 351–370. doi: 10.1016/j.chemgeo.2007.03.021

Haley, B. A., Klinkhammer, G. P., and McManus, J. (2004). Rare earth elements in pore waters of marine sediments. *Geochimica Cosmochimica Acta* 68, 1265–1279. doi: 10.1016/j.gca.2003.09.012

Henderson, G. M., Martel, D. J., O'Nions, R. K., and Shackleton, N. J. (1994). Evolution of seawater $^{87}Sr/^{86}Sr$ over the last 400 ka: the absence of glacial/interglacial cycles. *Earth Planet. Sci. Lett.* 128, 643–651. doi: 10.1016/0012-821X(94)90176-7

Hu, D., Clift, P. D., Boning, P., Hannigan, R., Hillier, S., Blusztajn, J., et al. (2013). Holocene evolution in weathering and erosion patterns in the Pearl River delta. *Geochem. Geophys. Geosyst.* 14, 2349–2368. doi: 10.1002/ggge.20166

Huang, K.-F., Blusztajn, J., Oppo, D. W., Curry, W. B., and Peucker-Ehrenbrink, B. (2012). High-precision and accurate determinations of neodymium isotopic compositions at nanogram levels in natural materials by MC-ICP-MS. *J. Anal. Atomic Spectrom.* 27, 1560–1567. doi: 10.1039/c2ja30123g

Huang, K. F., You, C. F., Chung, C. H., and Lin, I. T. (2011). Nonhomogeneous seawater Sr isotopic composition in the coastal oceans: A novel tool for tracing water masses and submarine groundwater discharge. *Geochem. Geophys. Geosys.* 12, Q05002. doi: 10.1029/2010GC003372

Huang, K.-F., You, C.-F., Chung, C.-H., Lin, Y.-H., and Liu, Z. (2014). Tracing the nd isotope evolution of north Pacific intermediate and deep waters through the last deglaciation from the south China sea sediments. *J. Asian Earth Sci.* 79, 564–573. doi: 10.1016/j.jseaes.2013.01.004

Jacobsen, S. B., and Wasserburg, G. J. (1980). Sm-Nd isotopic evolution of chondrites. *Earth Planet. Sci. Lett.* 50, 139–155. doi: 10.1016/0012-821X(80)90125-9

Jeandel, C., Arsouze, T., Lacan, F., Techine, P., and Dutay, J. (2007). Isotopic Nd compositions and concentrations of the lithogenic inputs into the ocean: A compilation, with an emphasis on the margins. *Chem. Geol.* 239, 156–164. doi: 10.1016/j.chemgeo.2006.11.013

Jonell, T. N., Clift, P. D., Hoang, L. V., Hoang, T., Carter, A., Wittmann, H., et al. (2017). Controls on erosion patterns and sediment transport in a monsoonal, tectonically quiescent drainage, song Gianh, central Vietnam. *Basin Res.* 29, S1, 659–683. doi: 10.1111/bre.12199

Lacan, F., and Jeandel, C. (2005). Neodymium isotopes as a new tool for quantifying exchange fluxes at the continent–ocean interface. *Earth Planet. Sci. Lett.* 232, 245–257. doi: 10.1016/j.epsl.2005.01.004

Laj, C. (2005). *MD 147 / MARCO-POLO1-IMAGESXII cruise, RV Marion Dufresne*. doi: 10.17600/5200050

Li, C.-F., Lin, J., Kulhanek, D. K.Expedition 349 Scientists (2015). *Proceedings of the international ocean discovery program*. (New York: International Ocean Discovery Program), 349. doi: 10.14379/iodp.proc.349

Li, C. S., Shi, X. F., Kao, S. J., Liu, Y. G., Lyu, H. H., Zou, J. J., et al. (2013). Rare earth elements in fine-grained sediments of major rivers from the high-standing island of Taiwan. *J. Asian Earth Sci.* 69, 39–47. doi: 10.1016/j.jseaes.2013.03.001

Li, X. H., Wei, G., Shao, L., Liu, Y., Liang, X., Jian, Z., et al. (2003). Geochemical and Nd isotopic variations in sediments of the South China Sea: a response to Cenozoic tectonism in SE Asia. *Earth Planet. Sci. Lett.* 211, 207–220. doi: 10.1016/S0012-821X(03)00229-2

Liu, Z., Colin, C., Huang, W., Le, K. P., Tong, S., Chen, Z., et al. (2007a). Climatic and tectonic controls on weathering in south China and IndoChina Peninsula: Clay mineralogical and geochemical investigations from the Pearl, Red, and Mekong drainage basins. *Geochem. Geophys. Geosys.* 8, Q05005. doi: 10.1029/2006GC001490

Liu, Z., Trentesaux, A., Clemens, S. C., Colin, C., Wang, P., Huang, B., et al. (2003). Clay mineral assemblages in the northern South China Sea: implications for East Asian monsoon evolution over the past 2 million years. *Mar. Geol.* 201, 133–146. doi: 10.1016/S0025-3227(03)00213-5

Liu, H. C., You, C. F., Chung, C. H., Huang, K. F., and Liu, Z. F. (2011). Source variability of sediments in the Shihmen Reservoir, Northern Taiwan: Sr isotopic evidence. *J. Asian Earth Sci.* 41, 297–306. doi: 10.1016/j.jseaes.2011.02.013

Liu, H. C., You, C. F., Huang, K. F., and Chung, C. H. (2012). Precise determination of triple Sr isotopes ($\delta^{87}Sr$ and $\delta^{88}Sr$) using MC-ICP-MS. *Talanta* 88, 338–344. doi: 10.1016/j.talanta.2011.10.050

Liu, Z., Zhao, Y. L., Colin, C., Stattegger, K., Wiesner, M. G., Huh, C. A., et al. (2016). Source-to-sink transport processes of fluvial sediments in the South China Sea. *Earth-Sci Rev.* 153, 238–273. doi: 10.1016/j.earscirev.2015.08.005

Liu, Z., Zhao, Y., Li, J., and Colin, C. (2007b). Late Quaternary clay minerals off Middle Vietnam in the western South China Sea: Implications for source analysis and East Asian monsoon evolution. *Sci. China Ser. D: Earth Sci.* 50, 1674–1684. doi: 10.1007/s11430-007-0115-8

Longman, J., Struve, T., and Pahnke, K. (2022). Spatial and temporal trends inmineral dust provenance in the SouthPacific—Evidence from mixing models. *Paleoceanogr. Paleoclimatol.* 37, e2021PA004356. doi: 10.1029/2021PA004356

Longman, J., Veres, D., Ersek, V., Phillips, D. L., Chauvel, C., and Tamas, C. G. (2018). Quantitative assessment of Pb sources in isotopic mixtures using a Bayesian mixing model. *Sci. Rep.* 8, 6154. doi: 10.1038/s41598-018-24474-0

Martin, E. E., Blair, S. W., Kamenov, G. D., Scher, H. D., Bourbon, E., Basak, C., et al. (2010). Extraction of Nd isotopes from bulk deep sea sediments for paleoceanographic studies on Cenozoic time scales. *Chem. Geol.* 269, 414–431. doi: 10.1016/j.chemgeo.2009.10.016

McLennan, S. M. (1989). Rare earth elements in sedimentary rocks: Influence of provenance and sedimentary processes. *Rev. Mineral.* 21, 169–200. doi: 10.1515/9781501509032-010

McManus, J. F., Francois, R., Gherardi, J.-M., Keigwin, L. D., and Brown-Leger, S. (2004). Collapse and rapid resumption of Atlantic meridional circulation linked to deglacial climate changes. *Nature* 428, 834–837. doi: 10.1038/nature02494

Meyer, I., Davies, G. R., and Stuut, J.-B. W. (2011). Grain size control on Sr-Nd isotope provenance studies and impact on paleoclimate reconstructions: An example from deep-sea sediments offshore NW Africa. *Geochem. Geophys. Geosys.* 12, Q03005. doi: 10.1029/2010GC003355

Milliman, J. D., and Farnsworth, K. L. (2011). *River Discharge to the CoastalOcean: A Global Synthesis* (Cambridge: Cambridge University Press), 384.

Mottl, M. J., Seewald, J. S., Wheat, C. G., Tivey, M. K., Michael, P. J., Proskurowski, G., et al. (2011). Chemistry of hot springs along the Eastern Lau Spreading Center. *Geochim. Cosmochim. Acta* 75, 1013–1038. doi: 10.1016/j.gca.2010.12.008

Nance, W. B., and Taylor, S. R. (1977). Rare earth element patterns and crustal evolution-II. archean sedimentary rocks from kalgoorlie, australia. *Geochim. Cosmochim. Acta* 41, 225–231. doi: 10.1016/0016-7037(77)90229-0

Nozaki, Y. (2000). "Rare Earth Elements and Their Isotopes," in *Encyclopedia of Ocean Sciences* (London: Academic Press).

Piotrowski, A. M., Goldstein, S. L., Hemming, S. R., and Fairbanks, R. G. (2004). Intensification and variability of ocean thermohaline circulation through the last deglaciation. *Earth Planet. Sci. Lett.* 225, 205–220. doi: 10.1016/j.epsl.2004.06.002

Pourmand, A., Dauphas, N., and Ireland, T. J. (2012). A novel extraction chromatography and MC-ICP-MS technique for rapid analysis of REE, Sc and Y: Revising CI-chondrite and Post-Archean Australian Shale (PAAS) abundances. *Chem. Geol.* 291, 38–54. doi: 10.1016/j.chemgeo.2011.08.011

Rutberg, R. L., Hemming, S. R., and Goldstein, S. L. (2000). Reduced North Atlantic Deep Water flux to the glacial Southern Ocean inferred from neodymium isotope ratios. *Nature* 405, 935–938. doi: 10.1038/35016049

Sang, P. N., and Liu, Z. (2021). Terrigenous sediment variations in the western South China Sea and their implications to East Asian monsoon evolution during the last glacial-interglacial cycle. *Quaternary Int.* 580, 1–10. doi: 10.1016/j.quaint.2021.02.008

Sang, P. N., Liu, Z., and Stattegger, K. (2019). Weathering and erosion in central Vietnam over the Holocene and Younger Dryas: Clay mineralogy and elemental geochemistry from the Vietnam Shelf, western South China Sea. *J. Asian Earth Sci.* 179, 1–10. doi: 10.1016/j.jseaes.2019.04.008

Sang, P. N., Liu, Z., Zhao, Y., Zhao, X., Pha, P. D., and Long, H. V. (2018). Chemical weathering in central Vietnam from clay mineralogy and major-element geochemistry of sedimentary rocks and river sediments. *Heliyon* 4, e00710. doi: 10.1016/j.heliyon.2018.e00710

Scher, H. D., and Delaney, M. L. (2010). Breaking the glass ceiling for high resolution Nd isotope records in early Cenozoic paleoceanography. *Chem. Geol.* 269, 329–338. doi: 10.1016/j.chemgeo.2009.10.007

Shao, L., Qiao, P., Pang, X., Wei, G., Li, Q., Miao, W., et al. (2009). Nd isotopic variations and its implications in the recent sediments from the northern South China Sea. *Chin. Sci. Bull.* 54, 311–317. doi: 10.1007/s11434-008-0453-8

Stock, B. C., Jackson, A. L., Ward, E. J., Parnell, A. C., Phillips, D. L., and Semmens, B. X. (2018). Analyzing mixing systems using a new generation of Bayesian tracer mixing models. *PeerJ* 6, e5096. doi: 10.7717/peerj.5096

Tachikawa, K., Athias, V., and Jeandel, C. (2003). Neodymium budget in the modern ocean and paleo-oceanographic implications. *J. Geophys. Res.* 108, 3254. doi: 10.1029/1999JC000285

Tachikawa, K., Jeandel, C., and Roy-Barman, M. (1999). A new approach to the Nd residence time in the ocean: the role of atmospheric inputs. *Earth Planet. Sci. Lett.* 170, 433–446. doi: 10.1016/S0012-821X(99)00127-2

Tan, M. T., Dung, L. V., Bach, L. D., Bieu, N., Nghi, T., Long, H. V., et al. (2014). Pliocene–Quaternary evolution of the continental shelf of central Vietnam based on high resolution seismic data. *J. Asian Earth Sci.* 79, 529–539. doi: 10.1016/j.jseaes.2013.08.001

Taylor, R., and McLennan, S. M. (1985). *The Continental Crust: Its Composition and Evolution* (Boston: Blackwell Scientific, Oxford).

Toyoda, K., Nakamura, Y., and Masuda, A. (1990). Rare earth elements of Pacific pelagic sediments. *Geochimica Cosmochimica Acta* 54, 1093–1103. doi: 10.1016/0016-7037(90)90441-M

Vinther, B. M., Clausen, H. B., Johnsen, S. J., Rasmussen, S. O., Andersen, K. K., Buchardt, S. L., et al. (2006). A synchronized dating of three Greenland ice cores throughout the Holocene. *J. Of Geophys. Res.* 111, D13102. doi: 10.1029/2005JD006921

von Blanckenburg, F. (1999). Tracing past ocean circulation? *Science* 286, 1862–1863. doi: 10.1126/science.286.5446.1862b

Wan, S., Toucanne, S., Clift, P., Zhao, D., Bayon, G., Yu, Z., et al. (2015). Human impact overwhelms long-term climate control of weathering and erosion in southwest China. *Geology* 43 (5), 439–442. doi: 10.1130/G36570.1

Wyndham, T., McCulloch, M., Fallon, S., and Alibert, C. (2004). High-resolution coral records of rare earth elements in coastal seawater: biogeochemical cycling and a new environmental proxy. *Geochimica Cosmochimica Acta* 68, 2067–2080. doi: 10.1016/j.gca.2003.11.004

Yang, S., and Youn, J.-S. (2007). Geochemical compositions and provenance discrimination of the central south Yellow Sea sediments. *Mar. Geol.* 243, 229–241. doi: 10.1016/j.margeo.2007.05.001

Yusof, A. M., Akyil, S., and Wood, A. K. H. (2001). Rare earth elements determination and distribution patterns in sediments of a polluted marine environment by instrumental neutron activation analysis. *J. Radioanal. Nucl. Chem.* 249, 333–341. doi: 10.1023/A:1013297932536

Zhang, Y., Lacan, F., and Jeandel, C. (2008). Dissolved rare earth elements tracing lithogenic inputs over the kerguelen plateau (Southern ocean). *Deep. Res. Part II Top. Stud. Oceanogr.* 55, 638–652. doi: 10.1016/j.dsr2.2007.12.029